# Position-Dependent Hydrophobicity of the Antimicrobial Magainin Peptide Affects the Mode of Peptide−Lipid Interactions and Selective Toxicity†

Tomoya Tachi,‡ Raquel F. Epand,§ Richard M. Epand,§ and Katsumi Matsuzaki*,‡

*Graduate School of Biostudies, Kyoto University, Sakyo-ku, Kyoto 606-8501, Japan, and Department of Biochemistry, McMaster University, Hamilton, Ontario, L8N 3Z5 Canada*

*Received February 19, 2002; Revised Manuscript Received June 27, 2002*

ABSTRACT: Cationic antimicrobial peptides are promising candidates as novel antibiotics of clinical usefulness. Magainin 2, a representative antimicrobial peptide isolated from the skin of the African clawed frog *Xenopus leavis*, electrostatically recognizes anionic lipids that are abundant in bacterial membranes, forming a peptide−lipid supramolecular complex pore, whereas the peptide does not effectively bind to zwitterionic phospholipids constituting the outer leaflets of mammalian cell membranes because of the low hydrophobicity of the peptide [Matsuzaki, K. (1999) *Biochim. Biophys. Acta 1462*, 1−10]. In this study, two magainin analogues with enhanced hydrophobicity, MG-H1 (GIKKFLHIIWKFIKAFVGEIMNS) and MG-H2 (IIKKFLHSIWKFGKAFVGEIMNI), with identical amino acid compositions were designed and interactions with lipid bilayers and biological activities were examined in comparison with those of MG (GIGKWLHSAKKFGKAFVGEIMNS = F5W-magainin 2). The apparent hydrophobicities and hydrophobic moments of MG-H1 and MG-H2, conventionally calculated assuming that all residues are involved in helix formation, were almost the same. MG-H2 behaved like MG except for greatly enhanced activity against zwitterionic membranes and erythrocytes. In contrast, despite a very similar calculated hydrophobicity, the observed hydrophobicity of MG-H1 was larger than that of MG-H2 because of a tendency toward helix fraying near the termini. Therefore, the physicochemical parameters of only the helical portion should be considered in characterizing peptide−lipid interactions, although this point was overlooked in most studies. Moreover, MG-H1 induced aggregation and/or fusion of negatively charged membranes. Furthermore, the peptide hydrophobicity was found to affect pore formation rate, pore size, and pore stability. These observations demonstrate that the hydrophobicity of the peptide also controls the mode of action and is dependent on the position of the hydrophobic amino acids in the peptide sequence.

A large number of antimicrobial peptides composed of 15−40 amino acids have been discovered in various organisms, including mammals, constituting host defense systems against invading pathogenic microorganisms (*1*). Broad antimicrobial spectra and highly selective toxicity make these compounds promising candidates as novel antibiotics of clinical usefulness (*2*). The selective toxicity is mainly due to preferential interactions of cationic peptides with anionic lipids, such as phosphatidylglycerol and lipopolysaccharides, abundantly present in bacterial membranes (*3*). The outer surfaces of mammalian cell membranes are almost exclusively composed of zwitterionic phospholipids, such as phosphatidylcholine and sphingomyelin, except for minor, negatively charged gangliosides. The major driving force of peptide binding to this class of membranes is hydrophobic interaction (*4*). The low hydrophobicity of antimicrobial peptides prevents strong binding to electrically neutral membranes. Therefore, hydrophobicity is an important determinant for cell selectivity.

Magainin 2 (GIGKFLHSAKKFGKAFVGEIMNS) is a representative antimicrobial peptide isolated from the skin of the African clawed frog *Xenopus leavis* (*5*−*7*). Our group has proposed the following model for magainin−lipid interactions. Magainin 2 selectively binds to anionic phospholipids, forming an amphipathic helix (*8*). Several helices form a toroidal pore (diameter of 2−3 nm) with surrounding lipids, inducing ion permeability and lipid flip-flop (*9*). Upon disintegration of the pore, a fraction of peptide molecules is stochastically translocated across the bilayer (*10, 11*). Using a series of magainin analogues, Dathe and colleagues pointed out that an increase in peptide hydrophobicity enhances membrane-permeabilizing activity against zwitterionic phosphatidylcholine membranes as well as erythrocytes (*12*). On the other hand, despite its sequence being similar to that of magainin 2, 18L[1] (GIKKFLGSIWKFIKAFVG), the archetype lytic peptide featuring the class L amphipathic α-helix (*13*), according to the classification of Segrest et al. (*14*), was reported to destabilize membranes, leading to the transient formation of large defects that result in contents leakage and, in the presence of bilayer−bilayer contact, could

† Supported by the Inamori Foundation, the Shimizu Foundation for the Promotion of Immunology Research, the Japan Securities Scholarship Foundation, and Grants-in-Aid for Scientific Research for an Advanced Area (13024244, 14017048, and 14572091) from the Ministry of Education, Culture, Sports, Science and Technology of Japan.

* To whom correspondence should be addressed. Telephone: 81 75 753 4574. Fax: 81 75 761 2698. E-mail: katsumim@pharm.kyoto-u.ac.jp.

‡ Kyoto University.

§ McMaster University.

10.1021/bi0256983 CCC: $22.00 
Published on Web 08/01/2002

lead to vesicle fusion (*15*). The 18L peptide is more hydrophobic than magainin 2. These observations suggest that changes in hydrophobicity can modulate not only lipid (cell) specificity but also the membrane permeabilization mechanism itself.

In this study, the 18L-like magainin analogue with enhanced hydrophobicity, MG-H1 (GIKKFLHIIWKFIKAFVGEIMNS), was designed, and interactions with lipid bilayers and biological activities were examined. Furthermore, MG-H2 (IIKKFLHSIWKFGKAFVGEIMNI) that has an amino acid composition identical to that of MG-H1 was also synthesized, and its properties were compared with those of MG (GIGKWLHSAKKFGKAFVGEIMNS = F5W-magainin 2) and MG-H1. The apparent hydrophobicities and hydrophobic moments of MG-H1 and MG-H2, conventionally calculated assuming that all residues are involved in helix formation, were almost the same. MG-H2 behaved like MG except for greatly enhanced activity against zwitterionic membranes and erythrocytes. In contrast, despite very similar calculated hydrophobicities, the experimentally observed hydrophobicity of MG-H1 was larger than that of MG-H2 because of a tendency toward helix fraying near the termini. Moreover, MG-H1 induced aggregation and/or fusion of negatively charged membranes. These observations demonstrate that the hydrophobicity of the peptide also controls the mode of action and is dependent on the position of introduction of hydrophobic amino acids.

## MATERIALS AND METHODS

*Materials*. The magainin analogues were synthesized by a standard fluoren-9-ylmethoxycarbonyl-based solid phase method, as described previously (*8*). The purity of the synthesized peptides was determined by analytical reversed phase high-performance liquid chromatography (RP-HPLC) and ion spray mass spectroscopy. Egg yolk L-α-phosphatidylcholine (PC), L-α-phosphatidyl-DL-glycerol enzymatically converted from PC (PG), egg yolk L-α-phosphatidylethanolamine (PE), trypsin, and fluorescein isothiocyanate dextrans (FITC-dextrans) (MW of 4400 and 42 000) were purchased from Sigma (St. Louis, MO). Egg yolk *N*-{[5-(Dimethylamino)naphthyl]-1-sulfonyl}-L-α-phosphatidylethanolamine (DNS-PE) and 1-palmitoyl-2-{6-[(7-nitrobenz-2-oxa-1,3-diazol-4-yl)amino]caproyl}-L-α-phosphatidylcholine ($C_6$-NBD-PC) were obtained from Avanti Polar Lipids (Alabaster, AL). Calcein was supplied by Dojindo (Kumamoto, Japan). Spectrograde organic solvents were obtained from nacalai tesque (Kyoto, Japan). All other chemicals from Wako (Tokyo, Japan) were of special grade. Tris-HCl buffer [10 mM Tris, 150 mM NaCl, and 1 mM EDTA (pH 7.4)] was prepared from NANOpure water (Barnstead, Dubuque, IA).

*RP-HPLC*. Chromatographic measurements were performed on a Shimadzu gradient HPLC system consisting of two LC-9A pumps, a manual injector, an SPD-6A UV spectrophotometric detector operating at 220 nm, and a C-R3A recorder. Analyses were carried out on a YMC-Pack R&D ODS column [250 mm × 4.6 mm (inside diameter), S-5 mm, 120A; YMC, Kyoto, Japan] at a flow rate of 1 mL/min at 30 °C. Mobile phase A was 0.1% trifluoroacetic acid in acetonitrile, and phase B was 0.1% trifluoroacetic acid in water. The retention times of the peptides were determined using a linear gradient from 10 to 90% B over the course of 40 min.

*Lipid Vesicles*. Large unilamellar vesicles (LUVs) were prepared and characterized as described elsewhere (*9*). Briefly, a lipid film, after drying under vacuum overnight, was hydrated with the desired solution and vortex-mixed to produce multilamellar vesicles (MLVs). The suspension was subjected to five freeze−thaw cycles and then extruded through polycarbonate filters (100 nm pore size filter, 21 times). Small unilamellar vesicles (SUVs) for circular dichroism (CD) measurements were produced by sonication of frozen and thawed MLVs in ice and water under a nitrogen atmosphere. The lipid concentration was determined in triplicate by phosphorus analysis (*16*).

*CD Spectra*. CD spectra were recorded at 30 °C on a Jasco J-720 apparatus interfaced with an NEC PC-9801 microcomputer, using a 1 mm path length quartz cell to minimize the absorbance due to the buffer component. The instrumental outputs were calibrated with nonhygroscopic ammonium *d*-camphor-10-sulfonate (*17*). Eight scans were averaged for each sample, and the averaged blank spectra were subtracted. The absence of any optical artifacts was confirmed as described elsewhere (*18*). The reported spectra are the averages of two independent preparations for each type of sample. Errors were within 5%.

*Tryptophan Fluorescence*. Fluorescence spectra in the range of 250−500 nm were measured at an excitation wavelength of 280 nm on a Shimadzu RF-5000 spectrofluorometer at 30 °C. The spectra were corrected for wavelength-dependent effects using a kit provided by the manufacturer after subtracting the corresponding blank spectra without the peptides. The reported spectra are the averages of two independent preparations for each type of sample. Errors were within 5%.

*Binding*. The partition coefficients for partitioning of the peptides into PC membranes were determined by a direct ultracentrifugation assay. Dry lipid films were hydrated with the peptides dissolved in NANOpure water at final peptide and lipid concentrations of 20 $\mu$M and 0−80 mM, respectively, vortex-mixed, and incubated overnight at 30 °C. After ultracentrifugation ($3.7 \times 10^5 \times g$ for 70 min), the free peptide concentrations in the supernatants were fluorometrically determined. In case the presence of trace amounts of lipids in the supernatant influenced Trp fluorescence, the peptide concentration was estimated after addition of SDS (final concentration of 20 mM). The pH values in the supernatants were 5.1 ± 0.1 and 4.1 ± 0.3 for MG-H1 and MG-H2, respectively.

[1] Abbreviations: CD, circular dichroism; CFU, colony-forming unit; $C_6$-NBD-PC, 1-palmitoyl-2-{6-[(7-nitrobenz-2-oxa-1,3-diazol-4-yl)amino]caproyl}-L-α-phosphatidylcholine; DNS-PE, egg yolk *N*-{[5-(dimethylamino)naphthyl]-1-sulfonyl}-L-α-phosphatidylethanolamine; DPoPE, dipalmitoleoyl-L-α-phosphatidylethanolamine; Fmoc, fluoren-9-ylmethoxycarbonyl; FITC-dextran, fluorescein isothiocyanate-bound dextran; 18L, GIKKFLGSIWKFIKAFVG; LUVs, large unilamellar vesicles; MG, GIGKWLHSAKKFGKAFVGEIMNS; MG-H1, GIKKFLHIIWKFIKAFVGEIMNS; MG-H2, IIKKFLHSIWKFGKAFVGEIMNI; MLVs, multilamellar vesicles; PC, egg yolk L-α-phosphatidylcholine; PE, egg yolk L-α-phosphatidylethanolamine; PG, L-α-phosphatidyl-DL-glycerol enzymatically converted from PC; *P*/*L*, peptide-to-lipid molar ratio; RET, resonance energy transfer; RP-HPLC, reversed phase high-performance liquid chromatography; SUVs, small unilamellar vesicles; $T_H$, lamellar-to-hexagonal II phase transition temperature.

*Calcein Leakage*. Membrane-permeabilizing activity was estimated by the extent of calcein leakage (*8*). Calcein-free LUVs were mixed with LUVs containing 70 mM calcein (pH adjusted to 7.4 with NaOH) to obtain the desired lipid concentration. The release of calcein from the LUVs was fluorometrically monitored at an excitation wavelength of 490 nm and an emission wavelength of 520 nm. The maximum fluorescence intensity corresponding to 100% leakage was determined by addition of 10% Triton X-100 (20 $\mu$L) to the sample (2 mL). The apparent percent leakage value was calculated according to

$$\% \text{ apparent leakage} = 100(F - F_0)/(F_t - F_0) \quad (1)$$

where $F$ and $F_t$ denote the fluorescence before and after addition of the detergent, respectively, and $F_0$ represents the fluorescence of the intact vesicles. In the leakage experiments using MG-H1, which aggregated in buffer, the peptide stock solution in water was diluted into buffer immediately (within 10 s) prior to each measurement. A longer incubation in buffer was confirmed to reduce leakage activity because of aggregate formation.

*FITC-Dextran Leakage*. The double-labeling method developed by our laboratory was utilized (*19*). DNS-PE (1.5 or 5 mol %)-containing LUVs entrapping 20 or 2 mM FITC-dextran (MW of 4400 or 42 000, respectively) were incubated with the peptide solution for 5 min. A 100 mg/mL trypsin solution (20 $\mu$L) was added to stop membrane permeabilization. The leaked FITC-dextran was removed by gel filtration using Bio-gel A-1.5m for FITC-dextran (MW of 4400) and Bio-gel A-15m for FITC-dextran (MW of 42 000). The excitation spectrum of the vesicle fraction after solubilization with Triton X-100 was measured at an emission wavelength of 520 nm. The percent leakage value was calculated as reported elsewhere (*19*).

*Pore Lifetime and Pore Formation Rate*. Pore lifetime, $\tau$, was evaluated by determining the extent of calcein self-quenching in the peptide-treated LUVs (*20*). After calcein-entrapped LUVs were mixed with the peptide solution, the time course of calcein fluorescence increase was monitored. Immediately after the apparent percent leakage value reached 60−90%, a 100 mg/mL trypsin solution (20 $\mu$L) was added to completely stop leakage. Aliquots of the liposome suspension (250 $\mu$L) were sampled. Triton X-100 was added to the rest of the liposome suspension to completely lyse the vesicles. The apparent retention, $E$, was calculated according to

$$E = (F_t - F)/(F_t - F_0) \quad (2)$$

On the other hand, the sampled liposomes were applied to a Bio-gel A-1.5m column to separate the vesicle fraction from leaked calcein, and its quenching factor ($Q$) was obtained by measuring the fluorescence intensity before ($F_b$) and after ($F_a$) the addition of Triton X-100.

$$Q = F_b/F_a \quad (3)$$

The $Q$ value was plotted against the $E$ value. The $\rho$ value, a dimensionless parameter describing the pore life span (*20*), was estimated from theoretical $Q$ versus $E$ curves for various $\rho$ values.

$$\rho = \tau_0/(\tau + \tau_0) \quad (4)$$

$\tau_0$ is the time necessary for a 1/$e$ reduction of the intravesicular dye concentration. The number of calcein-permeable pores formed per vesicle, $p$, was calculated according to eq 5.

$$p = -(\ln R)/(1 - \rho) \quad (5)$$

The true retention of the dye, $R$, was obtained from the apparent retention, $E$, by the method of Schwarz and Arbuzova (*20*).

*Peptide Translocation*. Resonance energy transfer (RET) from the Trp residue to the dansyl chromophore was utilized to monitor peptide binding. PG/PC/DNS-PE (40/50/10) LUVs (100 $\mu$L) were incubated with the peptide solution (1900 $\mu$L) at 30 °C. The binding of the peptide increases fluorescence due to RET. After incubation for 10 s, 30 s, 2 min, and 5 min, a 100 mg/mL trypsin solution (20 $\mu$L) was added to digest the untranslocated peptides, desorbing the fragments off the bilayers, which resulted in a decrease in dansyl fluorescence. For the control experiment, LUVs and trypsin were simultaneously added to the peptide solution. Sensitized dansyl fluorescence at 512 nm was recorded upon excitation of Trp at 280 nm. An increase in fluorescence after addition of trypsin, compared with fluorescence in the control experiment, implied the extent of the undigested, internalized peptides within the LUVs. The inner filter effects due to addition of trypsin were corrected.

*Lipid Flip-Flop*. The peptide-induced lipid flip-flop was determined as previously reported (*9*). NBD-labeled LUVs composed of PG, PC, and $C_6$-NBD-PC (50/49.5/0.5) were mixed with 1 M sodium dithionite and 1 M Tris ([lipid] = 10 mM and [dithionite] = 70 mM) and incubated for 15 min at 30 °C to produce inner leaflet-labeled vesicles. The vesicles were immediately separated from dithionite by gel filtration. The asymmetrically NBD-labeled LUVs were incubated with or without the peptide for various periods at 30 °C. The fraction of NBD-labeled lipids that had flopped during incubation was measured on the basis of fluorescence quenching by sodium dithionite. After the addition of the trypsin solution (100 mg/mL) to recover the barrier, 20 $\mu$L of a 1 M sodium dithionite/1 M Tris solution was added. Fluorescence was monitored at excitation and emission wavelengths of 460 and 530 nm, respectively.

*Antimicrobial Activity*. The minimum inhibitory concentrations of the peptides against *Escherichia coli* (ATCC 25922) were determined as described by Park et al. (*21*). The cells were cultured in 3% (w/v) trypticase soy broth at 37 °C overnight. To obtain cells in the mid-logarithmic phase, aliquots of 1 mL of the cultures were then transferred into 100 mL of fresh trypticase soy broth and incubated for 2−3 h. The cells were washed with cold 10 mM sodium phosphate buffer (pH 7.4) and resuspended in the same buffer. The cell concentrations were estimated by absorbance at 600 nm (CFU/mL = $A_{600} \times 8 \times 10^8$) and adjusted to $3.6 \times 10^6$ CFU/mL. The peptide samples (90 $\mu$L) were added to each well of 96-well plates. The inoculum (10 $\mu$L) was added and preincubated at 37 °C for 3 h. Trypticase soy broth (6%, 100 $\mu$L) was added and the mixture incubated at 37 °C for 12 h. Cell growth was assessed by the optical density at 600 nm on a Model 550 microplate reader (Bio-Rad, Hercules,

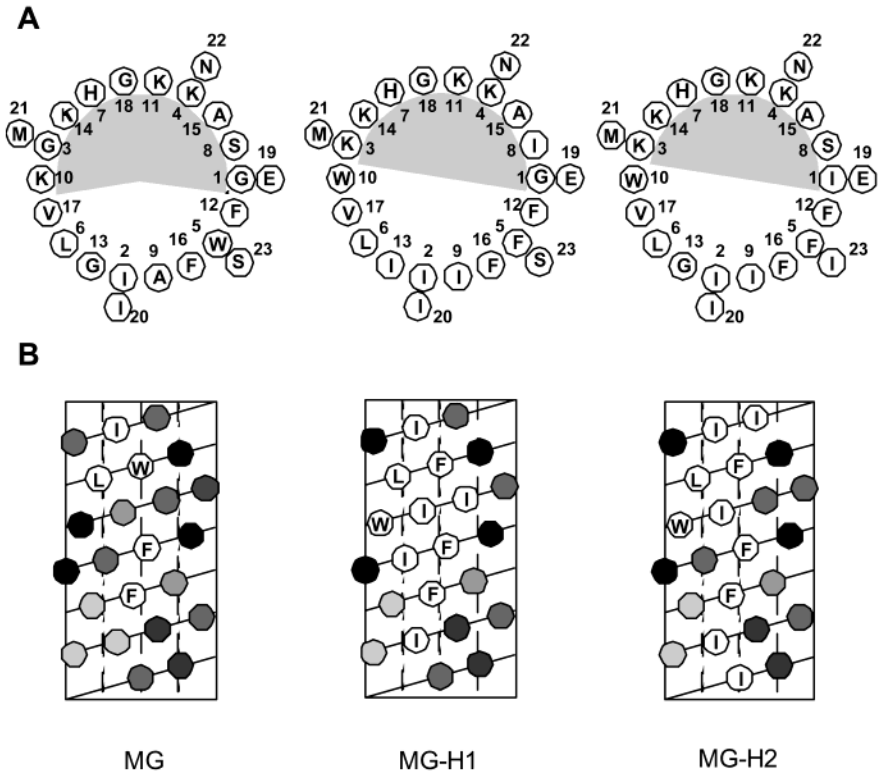


FIGURE 1: (A) Helical wheel representations of magainin analogues. The shaded areas represent the polar surface of the amphipathic helix. (B) Helical net representations. The hydrophobicity of each amino acid is represented in gray with the most polar residues in black.

CA). The minimum inhibitory concentration was defined as the lowest concentration of peptide that inhibited growth.

*Hemolytic Activity*. Human erythrocytes (blood type O) from a healthy 22-year-old man were freshly prepared prior to the experiments. The blood was centrifuged (800*g* for 10 min) and washed three times with PBS (pH 7.4) to remove plasma and the buffy coat. Erythrocyte specimens were kept on ice throughout. Various concentrations of peptides were incubated with the erythrocyte suspension [final erythrocyte concentration of 1% (w/v)] for 1 h at 37 °C. The percent hemolysis was determined from the optical density at 540 nm of the supernatant after centrifugation (800*g* for 10 min) (*3*). Hypotonically lysed erythrocytes were used as the standard for 100% hemolysis.

## RESULTS

*Peptide Design*. The hydrophobic magainin analogue MG-H1 (G3K/S8I/A9I/K10W/G13I-magainin 2) was designed by mimicking 18L [G3K/H7G/A9I/K10W/G13I-magainin 2 (1−18)]. The S8I mutation was introduced to devise the counterpart analogue MG-H2 (G1I/G3K/A9I/K10W/S23I-magainin 2) with the identical amino acid composition. Between the two analogues, there are only two differences in the positions of substitution, i.e., S8I and G13I versus G1I and S23I. As shown by the helical net representations (Figure 1), the hydrophobic residues are clustered in the central region of the sequence of MG-H1, whereas they are more evenly distributed along the sequence of MG-H2. The other calculated apparent physicochemical parameters such as the hydrophobicity and the hydrophobic moment of the entire sequence, the hydrophobicity of the putative nonpolar face, the charge, and the polar angle are almost the same in these molecules (Table 1). The Trp residue at the polar−nonpolar interface is useful for monitoring the polarity of the surroundings.

Table 1: Physicochemical Parameters of Magainin Analogues

| peptide | charge[a] | $H$ (kcal/mol)[b,e] | $H_{np}$ (kcal/mol)[c,e] | $\mu$[d,e] | $t_R$ (min)[f] | $K_{PC}$ ($M^{-1}$)[g] |
|---|---|---|---|---|---|---|
| MG | +3 | −9.1 | −12.6 | 0.488 | 17.6 | ND[h] |
| MG-H1 | +3 | −16.0 | −17.7 | 0.596 | 31.5 | 2200 ± 200 |
| MG-H2 | +3 | −16.0 | −17.7 | 0.607 | 21.7 | 210 ± 10 |

[a] Charges at physiological pH assuming that the α-$NH_2$ and His groups are protonated and deprotonated, respectively. [b] The summation of side chain hydrophobicities according to Fauche're and Pliska based on the octanol−water partitioning of individual *N*-acetyl amino acid residues (*28*). [c] The summation of side chain hydrophobicities on the nonpolar face. [d] Hydrophobic moment calculated following the Eisenberg formula (*35*) with the hydrophobic scale of Fauche're and Pliska (*28*). [e] These parameters are calculated assuming that all residues are involved in helix formation, as conventionally done. It should be noted, however, that these parameters do not exactly express those of the membrane-bound peptides, because both termini of the helix tend to be frayed. See the text for details. [f] RP HPLC retention time. [g] Partition coefficient from water to egg PC bilayers. [h] Not determined because of weak binding.

*Peptide Hydrophobicity*. A number of studies have showed that the RP-HPLC retention time is a measure of hydrophobicity of a membrane-acting peptide (*12*, *22*−*24*), although it is not fully established how peptides interact with the reverse phase in HPLC. The retention times were in the following order: MG-H1 ≫ MG-H2 > MG; this order suggests MG-H1 has an extremely hydrophobic character (Table 1). Indeed, MG-H2 and MG were soluble in buffer of physiological ionic strength at least up to 100 $\mu$M, whereas the solution of MG-H1 was turbid even at 0.5 $\mu$M, suggesting that MG-H1 formed large aggregates. CD spectra (Figure 2A) also showed that MG-H2 assumed an unordered conformation, whereas MG-H1 self-aggregated in buffer as

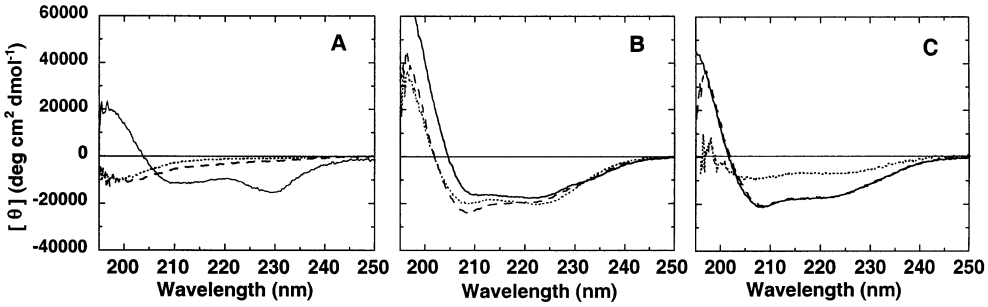


FIGURE 2: Secondary structures. CD spectra of the magainin peptides (25 $\mu$M) were recorded at 30 °C in (A) 10 mM Tris/150 mM NaCl/1 mM EDTA (pH 7.4) buffer, (B) 1 mM PG SUVs, and (C) 1 mM PC SUVs. In panels B and C, the spectra of MG-H1 were recorded in SUVs dispersed in water: (•••) MG, (—) MG-H1, and (− − −) MG-H2.

Table 2: Trp Emission Maxima (nm) of Magainin Analogues[a]

| peptide | buffer | water | PG/PC (1/1) | PC |
|---|---|---|---|---|
| MG | 349 ± 1 | ND[a] | 336 ± 1 | ND[b] |
| MG-H1 | 326 ± 1 | 346 ± 1 | 324 ± 1[c] | 327 ± 2[c] |
| MG-H2 | 348 ± 2 | 348 ± 2 | 330 ± 1[d] | 333 ± 2[d] |

[a] The peptide and lipid concentrations were 2 and 214 $\mu$M, respectively. [b] Not determined. [c] In water. [d] In buffer.

judged from the unusual spectral shape. The CD spectra of MG-H1 were independent of peptide concentration (2.5−50 $\mu$M), suggesting that the peptide was in similar aggregated states in this concentration range. The fluorescence spectra of the Trp residues further supported this conclusion (Table 2). The maximal emission wavelengths of MG-H2 and MG were 348−349 nm, typical for water-exposed Trp. In contrast, that of MG-H1 was significantly blue-shifted by 22 nm, indicating that the Trp residue was in a less polar environment because of self-aggregation. However, in pure water, where strong electrostatic repulsion between the Lys residues hampers peptide self-aggregation, MG-H1 was soluble and exhibited spectroscopic properties very similar to those of MG-H2 (Table 2). The CD spectrum of HG-H1 in water was typical of an unordered structure (spectrum not shown).

The binding affinities of these peptides for zwitterionic PC bilayers were measured in water, in which the peptides were completely soluble, by the direct ultracentrifugation method. Hydrophobic interactions play a major role in the binding of an amphipathic helix to electrically neutral membranes (*4*). The binding isotherms, i.e., the bound peptide per lipid (moles per mole) versus free peptide concentration (molar) plots, were almost linear up to a free peptide concentration of 6 $\mu$M because the bound peptide per lipid values were smaller than 0.01, where electrostatic repulsion between membrane-bound peptides was negligible. The slopes of the isotherms provided partition coefficients $K_{PC}$ summarized in Table 1. The $K_{PC}$ value of MG-H1 was 1 order of magnitude larger than that of MG-H2.

*Secondary Structures and Trp Fluorescence in Membranes*. The conformations of the peptides in bilayers were estimated by CD (Figure 2B,C). The spectra of MG-H1 were measured in water because the addition of SUVs precipitated MG-H1 in buffer. In the presence of PG or PC membranes, the peptides exhibited typical spectra of an α-helix with double minima around 208 and 222 nm (Figure 2B,C), indicating that the peptides bind to both PG and PC membranes. MG-H1 induced the aggregation of PG-containing vesicles (vide infra). The spectrum of MG-H1 in PG SUVs at shorter wavelengths differed from those of MG-H2 and MG probably because of light scattering. The binding of MG to PC membranes was not complete even at a lipid/peptide ratio of 40 because further addition of SUVs resulted in deeper double minima (data not shown). The other reported spectra corresponded to the membrane-bound form as judged from the observation that further addition of liposomes did not cause any additional changes in the spectra.

In the presence of PG/PC or PC LUVs, Trp fluorescence was blue-shifted by 13−22 nm (Table 2), suggesting that the Trp residues were in more hydrophobic environments. The extent of the blue shift was correlated with peptide hydrophobicity.

*Membrane Permeabilization*. Membrane permeabilization activity was examined on the basis of the efflux of a fluorescence dye, calcein, from LUVs of various lipid compositions. Figure 3A shows the time courses of leakage from PG/PC (1/1) LUVs. The dye release rate of MG (trace 1) decreased with increasing time, reflecting a pore deactivation process due to peptide translocation across membranes as reported previously (*10*). The MG-H2-induced leakage followed a similar time course (trace 3). In contrast, the addition of MG-H1 caused an initial abrupt leakage followed by a much slower leakage (trace 2). In addition, the change in 90° light scattering intensity of peptide-treated LUVs at 400 nm was monitored (Figure 3C). The addition of MG (trace 1) or MG-H2 (trace 3) did not change the light scattering intensity, indicating that neither micellization nor fusion of the liposomes occurred. In the case of MG-H1 (trace 2), the peptide treatment induced a rapid increase in the scattering intensity, suggesting that the MG-H1-induced permeabilization of PG/PC (1/1) bilayers accompanied aggregation and/or fusion of the vesicles.

Figure 3B shows the time courses of leakage from PC LUVs. MG exhibited much weaker leakage activity than MG-H1 and MG-H2, even at a 10-fold higher peptide concentration, reflecting weaker binding of MG to PC bilayers. The rate of dye leakage decreased with increasing time for MG-H2, whereas that of MG-H1 was almost constant. In both cases, no light scattering change was observed (data not shown).

*Dose−Response Curves and Effects of PE Incorporation*. Figure 4 shows the apparent percent leakage values at 5 min as a function of peptide-to-lipid molar ratio (*P*/*L*). The leakage activities of the three peptides against PG/PC (1/1) LUVs (empty symbols in Figure 4A) were comparable with each other. In contrast, MG-H1 and MG-H2 permeabilized PC bilayers more strongly than MG (empty symbols in

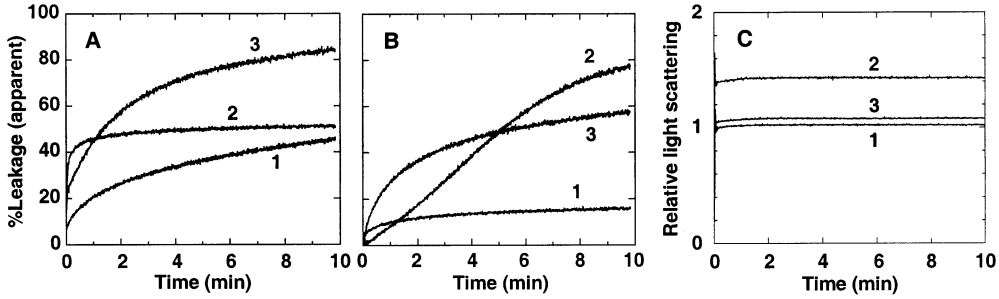


FIGURE 3: Kinetics of membrane permeabilization induced by the magainin peptides. The apparent percent calcein leakage values are plotted as a function of time. The lipid concentration was 52.5 $\mu$M. (A) Leakage from PG/PC (1/1) LUVs: trace 1, 1 $\mu$M MG; trace 2, 1 $\mu$M MG-H1; and trace 3, 1 $\mu$M MG-H2. (B) Leakage from PC LUVs: trace 1, 10 $\mu$M MG; trace 2, 1 $\mu$M MG-H1; and trace 3, 1 $\mu$M MG-H2. (C) The right angle light scattering intensity at 400 nm relative to the value of peptide-untreated vesicles was measured under the same conditions described for panel A.

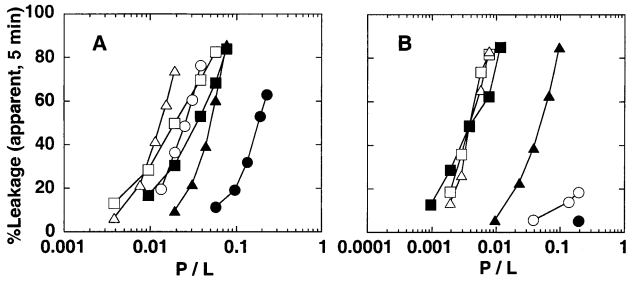


FIGURE 4: Dose−response curves for membrane permeabilization induced by the magainin peptides. The apparent percent calcein leakage values at 5 min for LUVs composed of (A) PG/PC (1/1) (empty symbols) and PG/PE (1/1) (filled symbols) and (B) PC (empty symbols) and PC/PE (1/1) (filled symbols) were plotted as a function of *P*/*L*. The lipid concentration was 52.5 $\mu$M: (○ and ●) MG, (□ and ■) MG-H1, and (△ and ▲) MG-H2. The temperature was 30 °C.

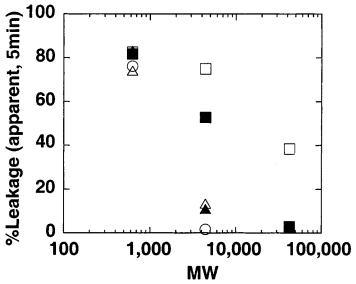


FIGURE 5: Estimation of pore size. The apparent percent calcein leakage values at 5 min of calcein (MW of 632), FITC-dextran (MW of 4400), and FITC-dextran (MW of 42 000) from PG/PC (1/1) LUVs (empty symbols) and PC LUVs (filled symbols) are plotted as a function of solute MW: (○ and ●) MG, (□ and ■) MG-H1, and (△ and ▲) MG-H2. The temperature was 30 °C.

Figure 4B) because of stronger binding. The incorporation of PE strongly inhibited the membrane permeabilization induced by MG and MG-H2 for both PG- and PC-based systems. In contrast, in the case of MG-H1, the presence of PE slightly decreased or hardly changed the leakage activity for the PG-based or PC-based system, respectively (filled symbols in Figure 4).

*Pore Size*. Leakage of three dyes of different sizes, i.e., calcein (MW of 623), FITC-dextran (MW of 4400), and FITC-dextran (MW of 42 000), was investigated to evaluate pore size (Figure 5). Under the conditions where 80% calcein leakage was observed, MG did not induce leakage of FITC-dextran (MW of 4400) from PG/PC (1/1) vesicles (○). MG-H2 triggered only slight leakage of the dye-labeled polymer from PG/PC (1/1) (△) and PC vesicles (▲). In contrast, the

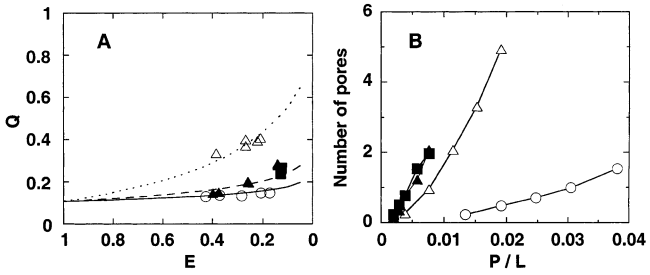


FIGURE 6: Pore lifetime and rate of pore formation. (A) The apparent calcein retention, *E*, is shown vs the quenching factor, *Q*. Theoretical curves for $\rho$ values of 0.1 (—), 0.2 (− − −), and 0.8 (···) calculated according to Schwarz and Arbuzova (*20*) are also shown. (B) The numbers of pores formed during 5 min were calculated from the dose−response curves for calcein release (Figure 3) and the pore lifetime data (Figure 5A) according to eq 5: (○ and ●) MG, (□ and ■) MG-H1, and (△ and ▲) MG-H2; empty symbols for PG/PC (1/1) vesicles and filled symbols for PC vesicles.

size of the MG-H1 pore (or defect) was larger than that of the other peptides, allowing a significant release of FITC-dextran (MW of 42 000) from PG/PC (1/1) LUVs (□) and FITC-dextran (MW of 4400) from PC LUVs (■).

*Pore Lifetime and Pore Formation Rate*. Pore lifetime was estimated on the basis of self-quenching of calcein according to the method of Schwarz and Arbuzova (*20*). The quenching factor (*Q*) of calcein is plotted against the apparent retention of calcein (*E*) in Figure 6A. The $\rho$ values were obtained by comparison of the data with the theoretical curves. For PG/PC (1/1) LUVs, the $\rho$ values of MG (○) and MG-H2 (△) were 0.1 ± 0.1 and 0.8 ± 0.1, respectively, corresponding to $\tau$ values of $9\tau_0$ and $0.25\tau_0$, respectively. For PC LUVs, the $\rho$ values of MG-H1 (■) and MG-H2 (▲) were both 0.2 ± 0.1, corresponding to a $\tau$ of $4\tau_0$.

As a measure of the rate of pore formation, the number of calcein-permeable pores formed per vesicle, *p*, during a 5 min period is shown in Figure 6B. The rate of pore formation of MG-H2 (△) was much larger than that of MG (○) in PG/PC (1/1) bilayers. In PC membranes, the pore-forming potency appeared to be very similar for MG-H1 (■) and MG-H2 (▲). We could not characterize pores in the MG-H1−PG/PC and MG−PC systems because of vesicle aggregation and weak interactions, respectively.

*Peptide Translocation*. Under the conditions where approximately 75% calcein leakage was observed over the course of 5 min, the translocation of MG (Figure 7A) and MG-H2 (Figure 7B) across PG/PC bilayers was detected on the basis of digestion of the untranslocated peptides by

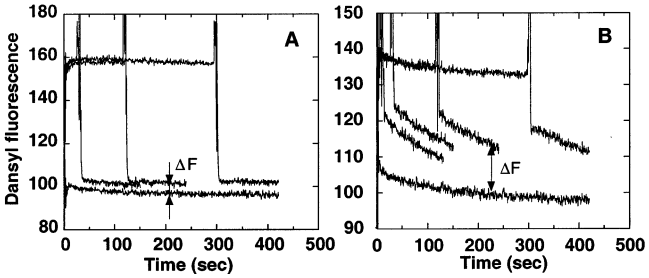


FIGURE 7: Detection of peptide translocation using RET. (A) MG (1.6 $\mu$M) or (B) MG-H2 (1 $\mu$M) was mixed with LUVs (52.5 $\mu$M) composed of PG/PC/DNS-PE (40/50/10) at 30 °C, and sensitized dansyl fluorescence at 512 nm was monitored at an excitation wavelength of 280 nm. Trypsin externally added at 10 s, 30 s, 2 min, and 5 min digested the untranslocated peptides, resulting in an abrupt decrease in fluorescence. The lowermost traces indicate the cases of no translocation with the enzyme added at time zero. $\Delta F$ is a measure of the extent of translocation.

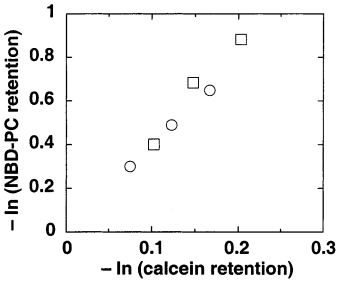


FIGURE 8: Coupling between pore formation and lipid flip-flop. Peptide-induced calcein leakage and lipid flip-flop were assessed using PG/PC (1/1) LUVs (52.5 $\mu$M) at 30 °C. The peptide concentrations were 1.6 and 1 $\mu$M for MG (○) and MG-H2, respectively. Relationships between the logarithms of the retention values of $C_6$-NBD-PC in the inner leaflets and calcein inside the vesicles are shown.

externally added trypsin. Trypsin was added to the peptide solution that had been incubated with dansyl-labeled vesicles for various periods. Simultaneous addition of trypsin and the vesicles to the peptide solution almost completely digested the peptide molecules and desorbed the fragments from the membranes within 20 s (the lowermost traces). Immediate cleavage of the peptide by the enzyme was also confirmed by the observation that calcein leakage was instantaneously stopped (data not shown). In contrast, prolonged preincubation protected the peptide from trypsin attack ($\Delta F$). Thus, the peptides were less sensitive to externally added trypsin at longer times, indicating that the peptide molecules translocated across the bilayers into the inner leaflets. Despite the lower concentration, MG-H2 translocated much more effectively than MG. The gradual decrease in dansyl fluorescence after trypsin addition in Figure 7B represents "back translocation" of the peptide from the inner to the outer leaflets.

*Lipid Flip-Flop*. As shown previously (*9*), the coupling between dye leakage and lipid flip-flop can be examined by comparison of ln(dye retention inside the vesicles) with ln(NBD-PC retention in the inner leaflets). MG and MG-H2 induced similar extents of lipid flip-flop in PG/PC LUVs, being coupled with dye leakage (Figure 8).

*Biological Activities*. Table 3 summarizes hemolytic activities against human erythrocytes and antimicrobial activities against *E. coli*. MG-H1 was 5-fold more hemolytic than MG-H2, whereas MG was practically nonhemolytic.

Table 3: Biological Activities of Magainin Analogues

| peptide | $ED_{50}$ ($\mu$M)[a] | MIC ($\mu$M)[b] | therapeutic index[c] |
|---|---|---|---|
| MG | >1000 | 8 | >125 |
| MG-H1 | 2.9 | 16 | 0.18 |
| MG-H2 | 16 | 2 | 8 |

[a] Peptide concentration at 50% lysis of human erythrocytes. [b] Minimum inhibitory concentration against *E. coli* (ATCC 25922). [c] $ED_{50}$/MIC.

An increase in hydrophobicity from MG to MG-H2 enhanced antibacterial activity 4-fold. The most hydrophobic MG-H1 exhibited an antibacterial activity even weaker than that of MG. That is, the therapeutic index was in the following order: MG ≫ MG-H2 ≫ MG-H1.

## DISCUSSION

*Hydrophobicity*. Structure−activity studies demonstrated that physicochemical parameters, such as hydrophobicity, hydrophobic moment, helicity, charge, and the angle subtended by the polar face, influence the action of an amphipathic α-helical peptide on model and biological membranes (*12*, *25*−*27*). The hydrophobicity of a polypeptide chain is usually calculated by the simple summation of the hydrophobicity of each constituent amino acid (side chain or whole residue), which is evaluated by various methods, including determination of the free energy of transfer of each amino acid from water to 1-octanol (*28*) or to lipid bilayers (*29*, *30*). This study clearly indicates that the simple summation of the hydrophobicity of each amino acid does not necessarily describe the hydrophobic properties of the peptide. Shifting the two Ile residues from the central region (the 8th and 13th positions) to the end of the sequences (the 1st and 23rd positions) markedly reduced hydrophobicity, as judged from the RP-HPLC retention time (Table 1), the solubility (Figure 2A and Table 2), and the affinity for PC (Table 1). The ratio of the $K_{PC}$ values gives a difference in $\Delta G$ of −1.4 kcal/mol at 30 °C. This difference is not due to different conformations because the CD spectra in egg PC bilayers were identical (Figure 2C). The helicities in PC (∼50%) were slightly smaller than that (60%) reported for magainin 2 amide (*4*). These low values suggested that the ends of the helices, especially when unblocked, tend to be frayed, and therefore, the Ile residues at the 1st and 23rd positions of MG-H2 do not appear to be fully involved in membrane binding. The double D-amino acid substitution experiments by Wieprecht et al. (*25*) concluded that magainin 2 amide forms a stable helix between residues 9 and 21, although it is difficult to exactly identify the residues involved in the helix by this indirect method. If all our magainin analogues also form helices between residues 9 and 21, the hydrophobicities of the putative helical parts are −11.4 and −9.6 kcal/mol for MG-H1 and MG-H2, respectively. The difference of −1.8 kcal/mol is close to the difference in free energy of PC partitioning (−1.4 kcal/mol).

The increase in hydrophobicity allowed deeper insertion of the helix into the hydrophobic cores of both types of bilayers. The maximal wavelength of Trp fluorescence of MG-H1 was more blue-shifted compared with those of MG-H2 and MG upon membrane binding (Table 2).

*Mechanisms of Membrane Permeabilization*. The 18L model peptide deteriorates the bilayer barrier property by imposing negative curvature strain on membranes (*15*). On

the other hand, magainin 2 increases the lamellar-to-hexagonal II phase transition temperature ($T_H$) of dipalmitoleoyl-L-α-phosphatidylethanolamine (DPoPE) (*31*), suggesting that the peptide imposes positive curvature strain on the membrane. The positive curvature stress leads to the formation of a peptide−lipid supramolecular complex pore (*9*, *32*). The following observations support this mechanism. The membrane permeabilization is coupled with peptide translocation and lipid flip-flop. The pore formed by magainin 2 has a measurable mean lifetime, size limit, and ion selectivity, and therefore, the average pore structure is better defined than mere membrane defects. Furthermore, in agreement with this view, pore formation was greatly inhibited by the incorporation of negative curvature-inducing PE into PG-based bilayers (*31*).

MG-H2 also induced lipid flip-flop (Figure 8) and translocated into the inner leaflet (Figure 7B) under the conditions where leakage occurred. The membrane permeabilization activity was remarkably reduced by the incorporation of PE (Figure 4). Furthermore, the pore formed by MG-H2 had a measurable mean lifetime and size limit (Figures 5 and 6). These observations suggest that MG-H2, like MG, forms a peptide−lipid supramolecular complex pore.

On the other hand, the MG-H1-induced permeabilization of PG/PC (1/1) membranes accompanied membrane aggregation and/or fusion (Figure 3C), suggesting that the mechanism of permeabilization of the PG-based bilayers by MG-H1 differs from those by MG and MG-H2. MG-H1 was designed as a model of 18L, which imposes negative curvature strain on membranes and decreases the $T_H$ of DPoPE (*13*). The 18L peptide induced the fusion and permeabilization of zwitterionic dioleoyl-L-α-phosphatidylcholine/dioleoyl-L-α-phosphatidylethanolamine membranes, and the extent of membrane permeabilization increased with the content of the phosphatidylethanolamine (*15*). In contrast, MG-H1 increased the $T_H$ of DPoPE (data not shown), and the incorporation of PE slightly inhibited its leakage activity against PG-based liposomes (Figure 4A). Therefore, MG-H1 appears to impose positive curvature strain on membranes in a manner similar to those of MG and MG-H2. However, the observations that MG-H1 induced fusion and/or aggregation of PG-based vesicles (Figure 3C) and the effects of PE incorporation were smaller than those of the other peptides indicate that MG-H1, penetrating deeper into membranes, also has some of the properties of negative curvature-imposing peptides.[2]

*Pore Characteristics*. The dimensions of calcein, FITC-dextran (MW of 4400), and FITC-dextran (MW of 42 000) as an oblate ellipsoid are approximately 1 nm × 2 nm, 2 nm × 4 nm, and 4 nm × 8 nm, respectively. With regard to PG/PC vesicles, the diameters of MG and MG-H2 pores are 2−3 nm, because FITC-dextran (MW of 4400) was almost impermeable (Figure 5). In contrast, the membrane defect induced by MG-H1 upon vesicle aggregation and/or fusion is large enough (>8 nm) to pass FITC-dextran (MW of 42 000) almost freely. Similarly, in PC bilayers, the pore formed by MG-H2 is not large enough for free leakage of FITC-dextran (MW of 4400). The MG-H1 pore could pass FITC-dextran (MW of 4400) freely but not FITC-dextran (MW of 42 000) at all; therefore, the size is 5−7 nm.

In the case of PG/PC bilayers, the lifetime of a MG-H2 pore was $0.25\tau_0$, whereas that of MG was $9\tau_0$ (Figure 6A). The $\tau_0$ value is inversely proportional to pore radius (*33*). The $\tau_0$ values for MG and MG-H2 are very similar because the pore sizes were similar (Figure 5). Therefore, the lifetime of the MG-H2 pore is ∼40 times shorter than that of MG. Furthermore, the pore formation of MG-H2 was faster than that of MG (Figure 6B). MG-H2 exhibited slightly higher overall membrane-permeabilizing activity than MG (Figure 4A) by forming pores much more frequently, compensating for the short pore lifetime. The faster translocation of MG-H2 (Figure 7) can be explained by faster pore formation and shorter pore lifetime, because peptide translocation occurs upon pore disintegration. The angles subtended by the polar face (*27*) and peptide charge (*34*) have been reported to modulate pore formation rate and pore lifetime, respectively. Our results suggest that peptide hydrophobicity also affects these properties.

In PC bilayers, $\tau = 4\tau_0$ for both the MG-H1 and MG-H2 pores. Considering the larger size of the MG-H1 pore (Figure 5), we conclude that the pore formed by MG-H1 with the largest hydrophobicity is less stable. In summary, a peptide with larger hydrophobicity tends to form a less stable, larger pore more frequently. The pore formation by MG-H2 was slightly facilitated in PC bilayers compared with that in PG/PC bilayers (Figure 6B), in keeping with the fact that PC with the more bulky headgroup has a greater tendency to impose positive curvature than PG.

The double-logarithmic plots of Figure 6B gave good linear relationships ($r > 0.992$) with similar slopes (1.5−1.8), suggesting that the number of peptide molecules in a pore is similar in the systems that were investigated (plots not shown).

*Biological Activities*. The differences in hydrophobicity also exhibited marked effects on cell selectivity (Table 3). Our magainin analogues with enhanced hydrophobicity were highly hemolytic compared with MG, which shows a very low affinity for phosphatidylcholine (*3*) and is practically nonhemolytic (Table 3). MG-H1 was 5-fold more hemolytic than MG-H2, in keeping with the differences in hydrophobicity and affinity for PC (Table 1).

In contrast to hemolytic activity, the antimicrobial activity was not strongly modulated by hydrophobicity (Table 3) because strong electrostatic interactions between the cationic peptides and the anionic bacterial membranes enabled complete membrane binding. The moderately different antimicrobial activities can be explained by the observations that the leakage activity of MG-H2 was higher against PG/PE membranes mimicking bacterial cell membranes than that of MG (Figure 4A). With regard to MG-H1, differences in the mode of action for anionic membranes as well as the self-aggregating property in buffer contribute to the lowest antimicrobial activity.

## CONCLUSION

The hydrophobicity of a small membrane-acting peptide, such as that forming a single helix, is usually calculated by the simple summation of the hydrophobicity of each constituent amino acid. Similarly, the hydrophobic moment is

[2] Incorporation of PE might reduce the level of peptide binding. However, the fact that MG-H1-induced leakage was not greatly inhibited by PE suggests that this effect was not so large.

conventionally evaluated by assuming that all residues are involved in secondary structure formation. A number of studies have discussed relationships between these apparent parameters and membrane activities (e.g., refs *12*, *23*, *24*, and *26*). However, our study using the magainin analogues clearly showed that the actual hydrophobicity of a peptide is affected by the position of introduction of hydrophobic amino acids; i.e., introduction of hydrophobic amino acids near the sequence termini makes a smaller contribution to the overall hydrophobicity than expected because of helix fraying. Therefore, to properly discuss the relationship between the physicochemical properties of a peptide and its membrane activity, those of the helix-forming part should be used instead of conventional calculations assuming the helix formation of the entire sequence.

An increase in the effective hydrophobicity results in an enhancement of the affinity of the peptide for zwitterionic phospholipids as well as for erythrocytes. In addition, the hydrophobicity controls pore properties. Thus, MG-H2, which is more hydrophobic and penetrates deeper into the hydrophobic core than the parent peptide MG, deforms the membrane more strongly, facilitating pore formation, whereas such a pore with large stress is less stable. Notably, an extreme increase in hydrophobicity changes the leakage mechanism, as shown for MG-H1. The deepest penetration of the peptide significantly expands the hydrophobic core of the bilayer, imposing effects of increased negative curvature, resulting in the aggregation and/or fusion of negatively charged vesicles and larger pores in zwitterionic membranes.

These results will be useful for the design of potent antimicrobial peptides.

## REFERENCES


1. Zasloff, M. (2002) *Nature 415*, 389−395.
2. Lohner, K. (2001) *Development of Novel Antimicrobial Agents: Emerging Strategies*, Horizon Scientific Press, Wymondham, U.K.
3. Matsuzaki, K., Sugishita, K., Fujii, N., and Miyajima, K. (1995) *Biochemistry 34*, 3423−3429.
4. Wieprecht, T., Beyermann, M., and Seelig, J. (1999) *Biochemistry 38*, 10377−10387.
5. Zasloff, M. (1987) *Proc. Natl. Acad. Sci. U.S.A. 84*, 5449−5453.
6. Matsuzaki, K. (1998) *Biochim. Biophys. Acta 1376*, 391−400.
7. Matsuzaki, K. (1999) *Biochim. Biophys. Acta 1462*, 1−10.
8. Matsuzaki, K., Murase, O., Tokuda, H., Funakoshi, S., Fujii, N., and Miyajima, K. (1994) *Biochemistry 33*, 3342−3349.
9. Matsuzaki, K., Murase, O., Fujii, N., and Miyajima, K. (1996) *Biochemistry 35*, 11361−11368.
10. Matsuzaki, K., Murase, O., Fujii, N., and Miyajima, K. (1995) *Biochemistry 34*, 6521−6526.
11. Matsuzaki, K., Murase, O., and Miyajima, K. (1995) *Biochemistry 34*, 12553−12559.
12. Wieprecht, T., Dathe, M., Beyermann, M., Krause, E., Maloy, W. L., MacDonald, D. L., and Bienert, M. (1997) *Biochemistry 36*, 6124−6132.
13. Tytler, E. M., Segrest, J. P., Epand, R. M., Nie, S.-Q., Epand, R. F., Mishra, V. K., Venkatachalapathi, Y. V., and Anantharamaiah, G. M. (1993) *J. Biol. Chem. 29*, 22112−22118.
14. Segrest, J. P., DeLoof, H., Dohlman, J. G., Brouillette, C. G., and Anantharamaiah, G. M. (1990) *Proteins: Struct., Funct., Genet. 8*, 103−117.
15. Polozov, I. V., Polozova, A. I., Tytler, E. M., Anantharamaiah, G. M., Segrest, J. P., Wooley, G. A., and Epand, R. M. (1997) *Biochemistry 36*, 9237−9245.
16. Bartlett, G. R. (1959) *J. Biol. Chem. 234*, 466−468.
17. Takakuwa, T., Konno, T., and Meguro, H. (1985) *Anal. Sci. 1*, 215−218.
18. Matsuzaki, K., Nakai, S., Handa, T., Takaishi, Y., Fujita, T., and Miyajima, K. (1989) *Biochemistry 28*, 9392−9398.
19. Matsuzaki, K., Yoneyama, S., and Miyajima, K. (1997) *Biophys. J. 73*, 831−838.
20. Schwarz, G., and Arbuzova, A. (1995) *Biochim. Biophys. Acta 1239*, 51−57.
21. Park, C. B., Kim, H. S., and Kim, S. C. (1998) *Biochem. Biophys. Res. Commun. 244*, 253−257.
22. Blondelle, S. E., and Houghten, R. A. (1992) *Biochemistry 31*, 12688−12694.
23. Kiyota, T., Lee, S., and Sugihara, G. (1996) *Biochemistry 35*, 13196−13204.
24. Castano, S., Desbat, B., and Dufourcq, J. (2000) *Biochim. Biophys. Acta 1463*, 65−80.
25. Wieprecht, T., Dathe, M., Schümann, M., Krause, E., Beyermann, M., and Bienert, M. (1996) *Biochemistry 35*, 10844−10853.
26. Wieprecht, T., Dathe, M., Epand, R. M., Beyermann, M., Krause, E., Maloy, W. L., MacDonald, D. L., and Bienert, M. (1997) *Biochemistry 36*, 12869−12880.
27. Uematsu, N., and Matsuzaki, K. (2000) *Biophys. J. 79*, 2075−2083.
28. Fauchere, J.-L., and Pliska, V. (1983) *Eur. J. Med. Chem. 18*, 369−375.
29. Wimley, W. C., and White, S. H. (1996) *Nat. Struct. Biol. 3*, 842−848.
30. Thorgeirsson, T. E., Russell, C. J., King, D. S., and Shin, Y.-K. (1996) *Biochemistry 35*, 1803−1809.
31. Matsuzaki, K., Sugishita, K., Ishibe, N., Ueha, M., Nakata, S., Miyajima, K., and Epand, R. M. (1998) *Biochemistry 37*, 11856−11863.
32. Ludtke, S. J., He, K., Heller, W. T., Harroun, T. A., Yang, L., and Huang, H. W. (1996) *Biochemistry 35*, 13723−13728.
33. Schwarz, G., and Robert, C. H. (1990) *Biophys. J. 58*, 577−583.
34. Matsuzaki, K., Nakamura, A., Murase, O., Sugishita, K., Fujii, N., and Miyajima, K. (1997) *Biochemistry 36*, 2104−2111.
35. Eisenberg, D., Weiss, R. M., and Terwilliger, T. C. (1982) *Nature 299*, 371−374.


BI0256983